Microscopic evidence of dimer breaking up in $CuO_2$ chain for Ca-substituted $Sr_{14}Cu_{24}O_{41}$ compounds



2007 J. Phys.: Condens. Matter 19 196224

(http://iopscience.iop.org/0953-8984/19/19/196224)

IOP PUBLISHING JOURNAL OF PHYSICS: CONDENSED MATTER

J. Phys.: Condens. Matter **19** (2007) 196224 (12pp) doi:10.1088/0953-8984/19/19/196224

# Microscopic evidence of dimer breaking up in $CuO_2$ chain for Ca-substituted $Sr_{14}Cu_{24}O_{41}$ compounds

**Jun Wang[1,2], Huamin Zou[1,2,3], Chao Guo[1,2], Lili Wang[1], Ni Hu[1] and Jing Shi[1]**

[1] Key Laboratory of Acoustic and Photonic Material and Device, Ministry of Education, Department of Physics, Wuhan University, Wuhan 430072, People's Republic of China
[2] Centre for Electron Microscopy, Wuhan University, Wuhan 430072, People's Republic of China

E-mail: hmzou@whu.edu.cn

Received 28 October 2006, in final form 29 March 2007
Published 20 April 2007
Online at stacks.iop.org/JPhysCM/19/196224

**Abstract**

In this work we measured the temperature dependence of the static magnetic susceptibility for Ca-doped $Sr_{14}Cu_{24}O_{41}$ compounds, studied the lattice mismatch between a $CuO_2$ chain and a $Cu_2O_3$ ladder by using electron diffraction, and found that the magnetic properties and lattice mismatch were sensitive to the Ca content. Applying a modified 'cut and projection' method, it is found that the lattice mismatch induces the dimers in spin chains to be decoupled into free spin $Cu^{2+}$. Further more, Ca doping makes lattice mismatch larger and more dimers decoupled. The number of dimerized spins and the number of free spins predicted by this method are in good agreement with those obtained by fitting the experimental static susceptibility data. This explanation can be applied not only to the Ca doping cases, but also to the case of oxygen nonstoichiometry.

## 1. Introduction

The spin-ladder compounds have attracted much attention since theoretical studies [1, 2] predicted that $S = 1/2$ one-dimensional antiferromagnetic Heisenberg chains can form a spin liquid state and have a spin gap in even-legged ladder structure. In particular, the series of compounds $(Sr, A)_{14}Cu_{24}O_{41}$ (A = Ca, Y, La, etc), which have a two-legged $Cu_2O_3$ ladder and a one-dimensional $CuO_2$ chain, have been studied extensively. In the series of compounds $Sr_{14-x}Ca_xCu_{24}O_{41}$, the average valence of Cu ions is +2.25, which means that there are six holes per formula unit (fu). They form self-doped systems. It is commonly considered that most holes are located in the $CuO_2$ chains in the $Sr_{14}Cu_{41}O_{41}$ pure compound [3]. When Sr in the compound is partially substituted by Ca, transfer of holes from the $CuO_2$ chain to the $Cu_2O_3$ ladder will occur. As Ca content increases, more holes transfer from the chain to the

[3] Author to whom any correspondence should be addressed.

  

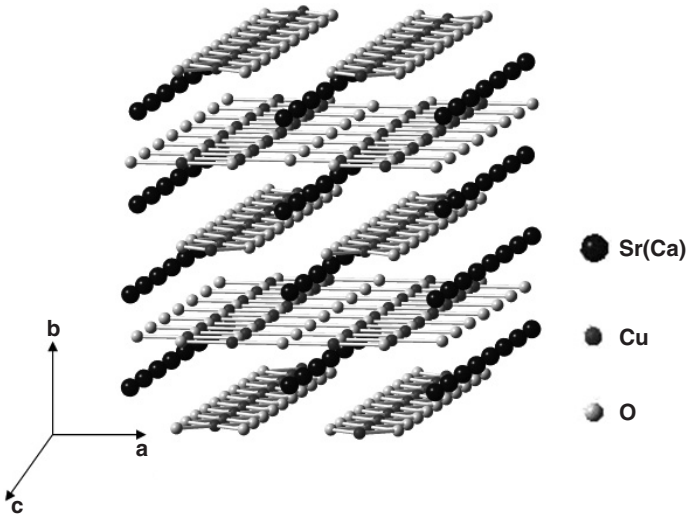


**Figure 1.** Incommensurate modulated structure of $(Sr, Ca)_{14}Cu_{24}O_{41}$.

ladder, and the electronic conductivity of the compound increases [4]. Under high pressure, an insulator-to-metal transition takes place in the highly Ca-doped phase, and superconductivity appears at low temperature [5, 6].

The series of compounds $Sr_{14-x}Ca_xCu_{24}O_{41}$ possesses a layered structure of two alternating substructures: a $Cu_2O_3$ ladder and a $CuO_2$ chain (figure 1) [7]. The layers of the first substructure consist of weakly coupled, two-leg spin ladders along the $\boldsymbol{c}$ direction. The spins in the ladder are strongly antiferromagnetically coupled on both legs and rungs, due to the 180° Cu–O–Cu bonds, while the interaction between ladders is very weak through 90° Cu–O–Cu bonds. Its space group is $Fmmm$. The second substructure is composed of a weakly coupled $CuO_2$ spin chain along the $\boldsymbol{c}$ direction. The spins in the chain are coupled via two 90° Cu–O–Cu bonds by the 3d orbital of the $Cu^{2+}$ ions. Its space group is $Fmmm$ (it is $Amma$ for the pure $Sr_{14}Cu_{24}O_{41}$). Sr (Ca) atoms sit between the two layers. Two substructures nearly have the same lattice parameters $\boldsymbol{a}$ and $\boldsymbol{b}$, but they have a large mismatch along the $\boldsymbol{c}$ direction. The ratio of $\boldsymbol{c}_L/\boldsymbol{c}_c$ is nearly 10/7 ($\boldsymbol{c}_L$ and $\boldsymbol{c}_c$ are the lattice parameters of the ladder and the chain, respectively, along the $\boldsymbol{c}$ direction). It has been shown that there is a strong correlation between the lattice mismatch and the physical properties [8, 9]. Hiroi *et al* [8] investigated the relationship between the misfit and the magnetic susceptibility as a function of oxygen nonstoichiometry. They pointed out that the lattice misfit along the $\boldsymbol{c}$ direction may induce a structure modulation in the chain, and this modulation will destroy the ideal charge order state that coincides with the superlattice period in the chain.

It is normally known that the magnetic properties below 300 K are mainly determined by the magnetic sequence of Cu ions (both $Cu^{2+}$ and $Cu^{3+}$) in the $CuO_2$ chain, and there is a strong relationship between the arrangement of Cu ions in the chain and the superlattice modulation, especially if doped with some ions, such as Ca, La, Y, etc [5]. The aim of this paper is to investigate the influence of Ca doping on the microstructure and the relationship between the microstructure and the magnetic properties. In the present study we measured the temperature dependence of the static magnetic susceptibility for a series of $Sr_{14-x}Ca_xCu_{24}O_{41}$ compounds, and deduced the number of dimerized spins $2N_D$ and the number of free spins $N_F$. We also investigated the structure of the compounds by means of electron diffraction. We found that the magnetic properties, as well as the superstructures, change with increasing Ca doping content, and that the ratio of $\boldsymbol{c}_L/\boldsymbol{c}_c$ is less than 10/7 for Ca doping. To explain this

**Table 1.** The atomic percentage of elements in $Sr_{14-x}Ca_xCu_{24}O_{41}$.

| Ca content ($X$) | Sr content (atom%) | Ca content (atom%) | Cu content (atom%) | O Content (atom%) |
|---|---|---|---|---|
| 0 | $18.23 \pm 2.32$ | 0.0 | $31.25 \pm 1.14$ | $50.52 \pm 4.00$ |
| 3.5 | $13.61 \pm 1.73$ | $4.54 \pm 0.22$ | $31.28 \pm 1.14$ | $50.57 \pm 4.00$ |
| 6.0 | $10.41 \pm 1.32$ | $7.80 \pm 0.37$ | $31.30 \pm 1.15$ | $50.49 \pm 4.00$ |
| 8.4 | $7.29 \pm 0.93$ | $10.93 \pm 0.53$ | $31.23 \pm 1.14$ | $50.55 \pm 4.00$ |

phenomenon we proposed a model which is based on the modified version of the 'cut and projection' method [10]. It shows that, as Ca content increases, the dimer will be decoupled into free spins $Cu^{2+}$ in the $CuO_2$ chain. This model gives a reasonable explanation between the observed superstructure and the magnetic properties.

## 2. Experiment

The samples were prepared by the standard solid-state reaction method. The starting materials were powders of $SrCO_3$ (99.0%), $CaCO_3$ (99.0%), and CuO (99%). The starting powders corresponding to $Sr_{14-x}Ca_xCu_{24}O_{41}$ ($x = 0, 3.5, 6, 8.4$) compositions were mixed uniformly by ball milling. The mixed powders were heated for 20 h at 1100 °C in air, and this process was repeated several times (more than three) with intermediate grindings until the impurity phases were undetectable. The reacted samples were then pulverized, pressed into pellets and sintered for 24 h at 940 °C in air [11].

Structure determination was carried out by powder x-ray diffraction analysis using a conventional diffractometer (Bruker AXS D8-Advance). It showed that the samples had a single phase. The temperature dependence of the static magnetic susceptibility was measured using a PPMS (Physical Property Measurement System) from 10 to 300 K under a magnetic field of 1 T. Electron diffraction experiments were performed in a JEOL JEM2010 (HT) microscope equipped with a Gatan 780 DualView CCD camera at room temperature. The accelerating voltage used was 200 kV. The electron diffraction patterns were recorded using the CCD camera, and the distances between any two diffraction spots were measured with Gatan DigitalMicrograph software.

The chemical compositions were measured using a GENSIS 700 EDAX at 20 kV in a Sirion FEG scanning electron microscope. Figure 2 shows the EDS spectra. The atomic percentages after ZAF correction are given in table 1. Because the fluorescence yield decreases with decreasing atomic number, and the mass absorption coefficients for low-energy x-rays are very large, the errors in quantitative EDS microanalysis of light elements ($Z < 11$) are quite large. Therefore, the oxygen percentages shown in table 1 mainly indicate that the oxygen contents in the four specimens are nearly equal. To obtain more a believable valence of the Cu ions, the core-level x-ray photoelectron emission spectra (XPS) of our samples were measured, as shown in figure 3. The main peak of Cu $2p_{3/2}$ is 933.8 eV, and the full width at half maximum height is 3.3 eV. By simulation of Cu $2p_{3/2}$ with XPSPEAK41, it is found that the percentages of $Cu^{2+}$ and $Cu^{3+}$ in our undoped sample $Sr_{14}Cu_{24}O_{41}$ are 92.13% and 7.87%, respectively. The average valence of Cu in this system is 2.08. No obvious change in the Cu 2p core-level induced by partially substituting Sr with Ca was observed. This confirms that the oxygen contents in the four samples are nearly equal. In the ideal compound $Sr_{14-x}Ca_xCu_{24}O_{41}$, the percentage of oxygen per formula is 51.90 atom%. From table 1, we can find that oxygen loss occurs by Ca substitution. This is in accordance with the results of other groups [5]. We chose four samples ($x = 0, 3.5, 6.0, 8.4$) with nearly identical oxygen content for the present study.

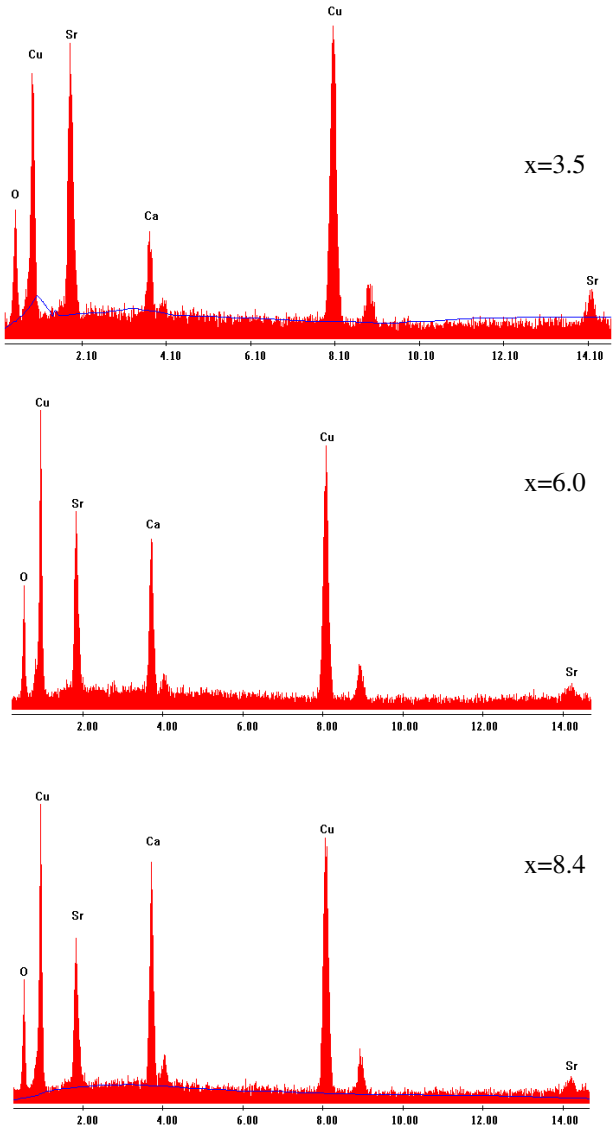


**Figure 2.** EDS spectra of $Sr_{14-x}Ca_xCu_{24}O_{41}$ compounds.

(This figure is in colour only in the electronic version)

## 3. Results

### *3.1. Magnetic susceptibility*

The temperature dependences of the magnetic susceptibility $\chi$ for different Ca-doped samples are shown in figure 4(a). The magnetic susceptibility increases as Ca content increases. For the sample with $x = 0$, $\chi$ exhibits a broad peak at 80 K and a Curie-like upturn is observed below 25 K. However, for the Ca-doped samples, the broad peak at 80 K becomes ambiguous, because the Curie–Weiss magnetic susceptibility increases with the Ca content. This result is in agreement with the result reported in [5]. The total magnetic susceptibility can be described as:

$$\chi_{\text{total}} = \chi_{\text{const}} + \chi_{\text{CW}} + \chi_{\text{chain}} + \chi_{\text{ladder}}. \quad (1)$$

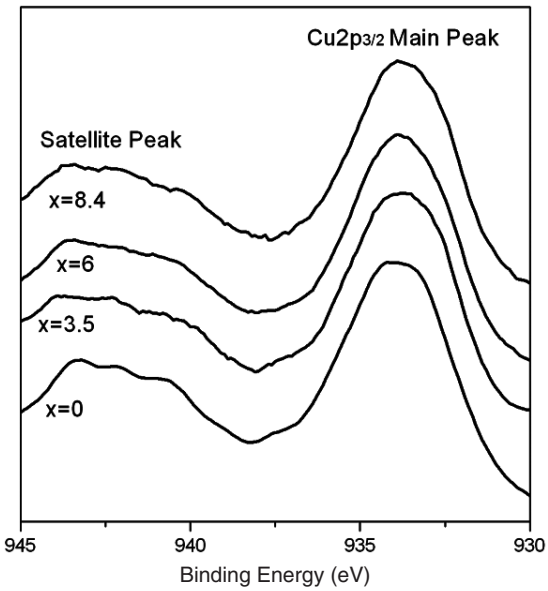


**Figure 3.** The core-level x-ray photoelectron emission spectra of $Sr_{14-x}Ca_xCu_{24}O_{41}$ compounds.

Here, $\chi_{const}$ is a temperature-independent term, $\chi_{CW}$ is a Curie–Weiss term, and $\chi_{chain}$ and $\chi_{ladder}$ are the magnetic susceptibilities of the spin chains and ladders, respectively. Because the term of $Cu_2O_3$ ladder has a large gap of 400 K [12], $\chi_{ladder}$ can be ignored in the range of observation temperature. $\chi_{CW}$ comes from the contribution of the free spin $Cu^{2+}$/fu, and $\chi_{chain}$ can be described with the independent spin-dimer model $\chi_{dimer}$. So the formula becomes:

$$\chi_{total} = \chi_{const} + \chi_{CW} + \chi_{dimer} \tag{2}$$

where $\chi_{CW}$ and $\chi_{chain}$ are:

$$\chi_{CW} = C/(T - \Theta) \tag{3}$$

$$C = N_F(N_A/24)g^2\mu_B^2/4k_B \tag{4}$$

$$\chi_{dimer} = 2N_D(N_A/24)g^2\mu_B^2/\{k_BT[3 + \exp(J_D/k_BT)]\}. \tag{5}$$

Here, $C$ is the Curie coefficient, $N_A$ is Avogadro's number, the Landé $g$-factor is 2.2 for $Cu^{2+}$, and $k_B$ and $\Theta$ are the Boltzmann constant and Weiss temperature, respectively. $J_D$ is the dimer coupling constant. $N_F$ is the number of free spins $Cu^{2+}$/fu, and $N_D$ is the number of dimers per fu.

Using equation (2) in fitting the $\chi \sim T$ curve for every sample, we obtained the values of $\Theta$, $J_D$, $N_F$, $N_D$ as shown in table 2. The Weiss temperature is negative. The number of free spin $Cu^{2+}$ increases, and the number of dimers $N_D$ decreases with increasing Ca content, while the measured whole number $2N_D + N_F$ is nearly constant (about 3.80 per fu), as shown in figure 4(b). It is also found from table 2 that the dimer coupling constant $J_D$ decreases, and the absolute value of Weiss temperature increases as the dimers are getting decoupled into free spins by Ca doping and the free spins begin seeing each other, which makes the antiferromagnetic interaction in $CuO_2$ chains increase slightly. For the ideal composite, $2N_D + N_F$ is 4.0. This difference in the value $2N_D + N_F$ (3.80) of the present Ca-doped samples from 4.0 of the idea compound may be due to the fact that the loss of oxygen induces a small nonstoichiometry in the contents of metal elements.

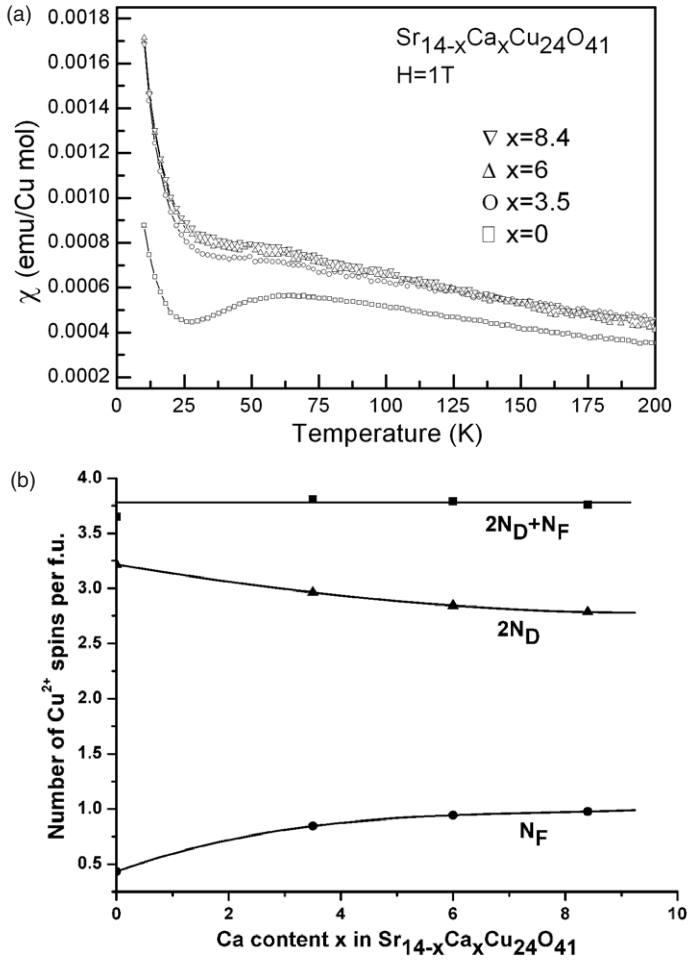


**Figure 4.** (a) Temperature dependence of static magnetic susceptibility, $\chi$, for the different Ca-doped samples. The solid line is a fit to equation (2) described in the text. (b) Dimerized spins per fu, $2N_D$, and free spins, $N_F$, as a function of the Ca content. The curves in the figure are drawn as a guide to the eye.

**Table 2.** Fitting result induced from equation (2).

| | $\Theta$ (K) | $J_D$ (K) | $N_F$ | $N_D$ | $N_F + 2N_D$ |
|---|---|---|---|---|---|
| $X = 0$ | $-0.52 \pm 0.12$ | $131.0 \pm 0.3$ | $0.432 \pm 0.001$ | $1.609 \pm 0.001$ | $3.650 \pm 0.003$ |
| $X = 3.5$ | $-0.80 \pm 0.17$ | $125.3 \pm 1.3$ | $0.845 \pm 0.001$ | $1.482 \pm 0.003$ | $3.809 \pm 0.007$ |
| $X = 6.0$ | $-1.20 \pm 0.29$ | $123.4 \pm 1.4$ | $0.943 \pm 0.003$ | $1.422 \pm 0.004$ | $3.787 \pm 0.011$ |
| $X = 8.4$ | $-1.98 \pm 0.21$ | $122.8 \pm 1.0$ | $0.977 \pm 0.002$ | $1.393 \pm 0.003$ | $3.763 \pm 0.008$ |

### *3.2. Electron diffraction analysis*

The structure determined by x-ray diffraction is the average structure in a volume with a diameter of 0.1 mm at least. Electron microscopy methods, such as electron diffraction and high-resolution image, can provide complementary information on local structures. In particular, for the incommensurate composite crystal, it will be easier to obtain the lattice

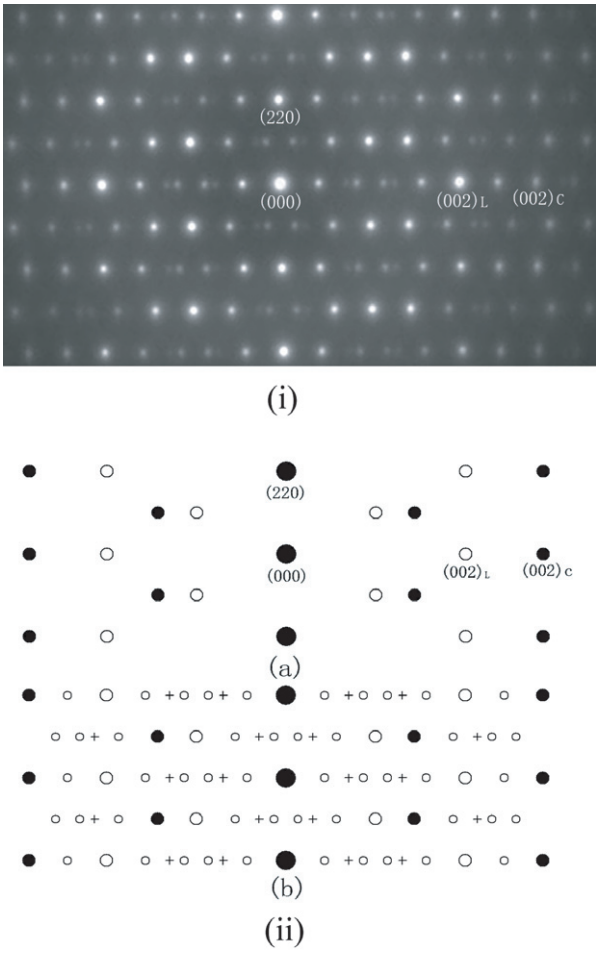


**Figure 5.** (i) [1$\bar{1}$0] zone axis electron diffraction pattern (EDP) for $x = 6.0$ sample. (ii) Sketches of the [1$\bar{1}$0] zone axis EDP. Picture (a) is the simulation with kinematical approximation of electron diffraction. Picture (b) shows the effect of multiple diffraction, which accords with experimental picture. In the sketches, middle open circles and middle full circles are from ladders and chains, respectively, large full circles are common to both sublattices, small open circles indicate double diffraction, and crosses indicate triple diffraction.

mismatch using the electron diffraction method [13]. In a [1$\bar{1}$0] zone axis electron diffraction pattern (EDP) for the sample with $x = 6.0$, as shown in figure 5(i), there are a lot of interesting spots in the picture. Figure 5(ii)(a) shows a simulated [1$\bar{1}$0] EDP with kinematical approximation of electron diffraction. Figure 5(ii)(b) shows the EDP as the multiple diffraction effect is taken into account, which accords with the experiments very well. The smaller and darker spots in figure 5(i) result from the multiple diffraction effect. If the lattice has a small change, the small spots (especially the triple diffraction spots) will move, though the main spots may not be changed obviously. Figure 6 shows two [1$\bar{1}$0] zone axis EDPs for the samples with different Ca contents. It is easier to see the difference between the two pictures from the enlarged parts. This indicates that the distance between the weak spots is very sensitive to the misfit of the two sublattices.

To estimate the magnitude of the lattice mismatch, we can define a parameter $\alpha$:

$$\alpha = c_{\mathrm{L}}/c_{\mathrm{c}}. \tag{6}$$

Assuming that the two sublattices match each other in the ideal compound $Sr_{14}Cu_{24}O_{41}$ with $\alpha = 10/7$, the difference between the $\alpha$ of a Ca-doped compound and the ideal value of 10/7 indicates the lattice mismatch. By measuring the distance between weak spots in the [1$\bar{1}$0] zone axis EDPs of the compounds, we can obtain the values of $\alpha$ for each view field of the samples.

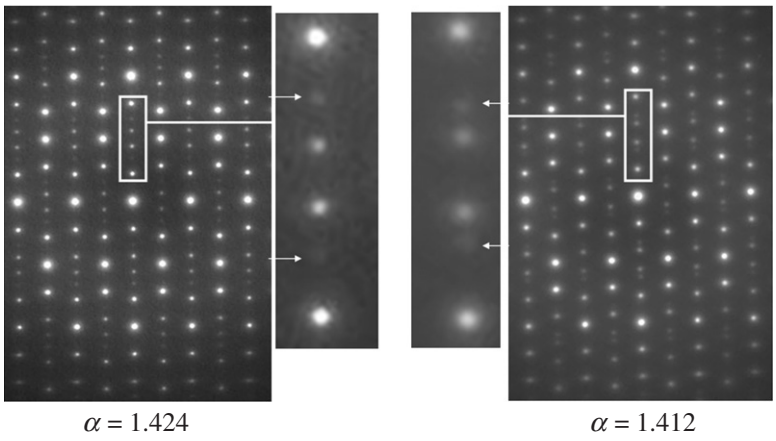


**Figure 6.** [$1\bar{1}0$] zone axis EDPs of $Sr_{14-x}Ca_xCu_{24}O_{41}$ compounds: $x = 0$ (left) and $x = 6$ (right).

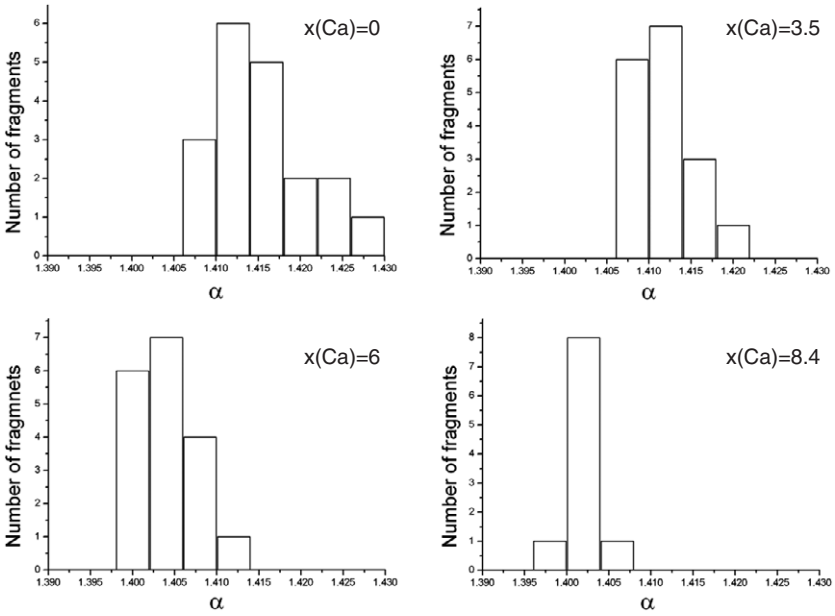


**Figure 7.** The statistic distribution of the $\alpha$ for different Ca content.

For each sample with $x = 0, 3.5, 6.0$, and 8.4 we chose 17 to 20 different areas for measuring $\alpha$. The results of the measurements are shown as the statistic histograms in figure 7. The measured $\alpha$ values range from 1.430 to 1.40. As Ca content increases, the value of $\alpha$ decreases, but the tendency becomes slow.

It is noticed that the measured $\alpha$ values of $Sr_{14}Cu_{24}O_{41+\delta}$ with $\delta = 0$ by Hiroi *et al* [8] ranged from 1.41 to 1.445 with a peak at 1.437, and the value of $\alpha$ increases as the oxygen content decreases. For our undoped sample, the oxygen content 50.52 atom% is less than the oxygen content 51.90 atom% of the ideal compound $Sr_{14}Cu_{24}O_{41}$, while the value of $\alpha$ of our undoped sample is about 1.42 with a small distribution, which is smaller than 1.437. This is inconsistent with the prediction of [8]. This discrepancy may be due to the following

factors. First, the mismatch is related not only to the density of holes but also to oxygen defects. The differences in the sample preparations may produce the inconsistency in the results of mismatch. Second, in [8], the $c$ parameters of the two sublattices were measured on negatives. We measured the $c$ parameters in digital diffraction patterns by using Gatan DigitalMicrograph software. The difference in measuring methods may also induce some difference in the results. Third, as is pointed out by Milat *et al* [14], the ratio of the sublattice parameters, $c_L/c_C$, is incommensurate and very close to $\sqrt{2}$ (=1.414...), which favours the assumption that the building unit, square planar $CuO_4$, is distorted very little in the ladders as well as in the chains. Fourth, assuming all holes to be in the chains, the average interatomic distance in the chains should decrease with increasing hole density. The hole density should decrease as the oxygen content decreases. This means that the lattice parameter $c_C$ should increase, and thus $c_L/c_C$ should decrease, as oxygen content decreases. Therefore, the result that the parameter $\alpha$ of our undoped sample is smaller than the value of $\alpha$ for the samples of $Sr_{14}Cu_{24}O_{41}$ in [8] is reasonable.

## 4. Discussion

In $Sr_{14}Cu_{24}O_{41}$ compound, since the positions of Cu ions in the $CuO_2$ chain can be influenced by the electrostatic potential of $Sr^{2+}$ ions, which has a period of $c_L/2$ in the ladder, some Cu–Cu bonds are elongated, and some shortened, in order to let Cu ions stay in the extremum points of the electrostatic potential. Because of this kind of modulation, there are dimers in the chains [8]. When $Ca^{2+}$ ions replace $Sr^{2+}$ ions, even if the $Ca^{2+}$ sit precisely at the positions of former $Sr^{2+}$ ions, the Cu ions in the chain should be influenced differently due to the difference between the electrostatic potential of the $Ca^{2+}$ ions and that of $Sr^{2+}$ ions. This will induce differences in the superstructure and physical properties. Hiroi *et al* [8] studied the relationship between the lattice misfit and magnetic susceptibility for oxygen nonstoichiometrical samples. According to their results that the oxygen deficiency makes the lattice mismatch $\alpha$ greater than 10/7, Hiroi *et al* [8] predicted that the $\alpha$ of Ca-doped samples should be larger than 10/7, because Ca doping induces oxygen deficiency. However, our experiments show that $\alpha$ is less than 10/7 for Ca-doped samples. This means that the effect of Ca doping on the lattice mismatch and the magnetic properties has to be taken into account, besides the effect of oxygen deficiency. Also, according to Hiroi's model, this situation ($\alpha < 10/7$) would result in a decrease of free spins, $N_F$, and an increase of dimers, $N_D$, in $CuO_2$ chains, which is in contradiction with the results shown in figure 4(b) and table 2. Therefore, we proposed a modification to Hiroi's model to explain the phenomena for Ca-doped compounds.

We use a modified 'cut and projection' method [10] to study the incommensurate structure. The two-dimensional (2D) orthogonal lattice is constructed with two characteristic lengths $l = 3\sqrt{2}c_c$ and $s = 2\sqrt{2}c_c$ (figure 8), and the one-dimensional (1D) sequence of segments $L = l/\sqrt{2} = 3c_c$ and $S = s/\sqrt{2} = 2c_c$ can be obtained by projecting the zigzag line within the strip onto a line $P$ with a slope of $\tan 45°$. This particular angle ensures that the lengths of the $L$ and $S$ segments remain unchanged in different projections. Then, the slope of a line passing through two lattice nodes is [8]:

$$\tan\theta = \frac{2}{3} \times \frac{6 - 4\alpha}{3\alpha - 4}$$

where $\alpha = c_L/c_c$. In the model of Hiroi *et al* [8], a single $S$ segment means dimer $\langle\uparrow\downarrow\rangle$, and the excess unpaired longer segment $L$ in the alternating $LS$ segment series produce free spin $Cu^{2+}$. This is based on the consideration that, due to the modulation of the ladder, two neighbouring Cu atoms with an increased distance appear, separated by three Cu atoms with

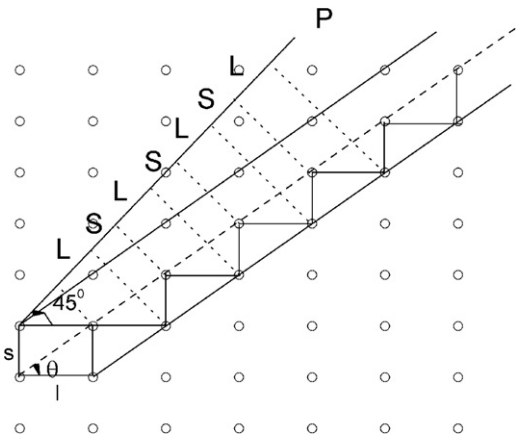


**Figure 8.** Modified version of the cut and projection method describing a uniform sequence of $L$ and $S$. This is the ideal case of $\alpha = 10/7$. The sequence produced by cut and projection is $LSLSLS\ldots$. Here single $L$ and $S$ means the segments containing three and two Cu ions, respectively, and $LS$ means a full magnetic series $\uparrow 0 \downarrow 00$ containing a dimer.

decreased bond lengths in the $CuO_2$ chain. Also, $Cu^{2+}$ must prefer the expanded positions, because it has a longer radius than $Cu^{3+}$. The two neighbouring $Cu^{2+}$ form a pair at dimerized sites. Then the dimer is $\langle\uparrow\downarrow\rangle$. However, some other experimental measurements, such as a nuclear magnetic resonance (NMR) study by Takigawa *et al* [15], neutron inelastic scattering by Regnault *et al* [16], x-ray diffraction by Gotoh *et al* [17] etc, indicated that the $\langle\uparrow\ 0\ \downarrow\rangle$ arrangement forms a dimer. Although there are several arguments for these, there is a common point, i.e. every five Cu ions contain one dimer, and the excess Cu ions are nonmagnetic Cu ions. Secondly, according to the result of Gotoh *et al* [17], in the series of compounds $Sr_{14-x}Ca_xCu_{24}O_{41}$, there are six holes per fu, and it is normally considered that nearly all the six holes are located in the chain. Because of the large Hubbard correlation of 3d electrons of the $Cu^{2+}$, the holes are mainly located near the oxygen, and are coupled with the nearby $Cu^{2+}$ ions to form nonmagnetic Zhang–Rice singlets [15]. For the ideal compounds of $\alpha = 10/7$, the magnetic series in $CuO_2$ chains is:

$$\uparrow 0 \downarrow 00 \quad \uparrow 0 \downarrow 00 \ldots$$

where $\uparrow, \downarrow$ are the signs of $Cu^{2+}$ spin with opposite directions, respectively, and 0 denotes the nonmagnetic Zhang–Rice singlet. Each two spin $Cu^{2+}$ ions are separated by one or two Zhang–Rice singlets. Two nearby spin of $Cu^{2+}$ ions with one Zhang–Rice singlet in the middle compose a dimer in the chain, namely $\langle\uparrow\ 0\ \downarrow\rangle$. It should be noted that it is not important to say where the chain starts and where the chain ends for a long chain. Therefore, the magnetic series in $CuO_2$ chain can be written as:

$$00 \uparrow 0 \downarrow \quad 00 \uparrow 0 \downarrow \quad \ldots$$

or

$$0 \downarrow 00 \uparrow \quad 0 \downarrow 00 \uparrow \quad \ldots$$

etc.

Therefore, unlike Hiroi's model [8] in which the short segment $S$ $(=2c_C)$ and the long segment $L$ $(=3c_C)$ represent dimer and trimer respectively, in the present model it is supposed that a single $L$ or $S$ segment only represents three or two positions for Cu ions, and a pair of $L$ and $S$ means five Cu ions that contains a dimer and the remains are nonmagnetic Cu ions. For the ideal crystal $\alpha = 10/7$, as shown in figure 8, the sequence is:

$$LSLSLSLS\ldots.$$

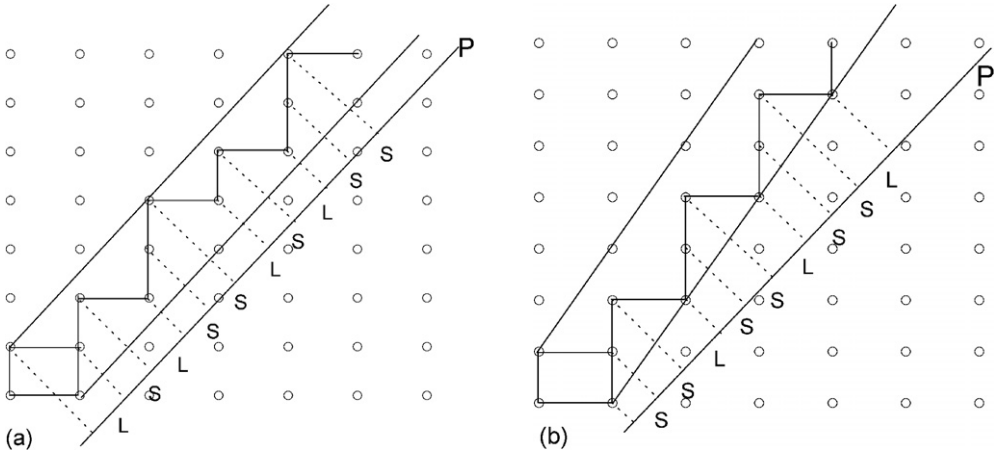


**Figure 9.** (a) The cut and projection picture for $\alpha = 24/17$; every two $LS$ pairs are followed by an $S$ segment. (b) The cut and projection picture for $\alpha = 7/5$; every $LS$ is followed by an $S$ segment.

Obviously, $2N_D = 4.0$ and $N_F = 0.0$ for the ideal case. For the case of $\alpha = 24/17$, as shown in figure 9(a), the sequence is $LSLSSLSLSS\ldots$, in which every two $LS$ pairs are followed by an $S$ segment. This means that every 12 Cu ions have $3.8 \times 12/10 = 4.56$ $Cu^{2+}$ (figure 4(b) shows that there are 3.8 $Cu^{2+}$ per fu, i.e. each ten $c_c$ have 3.8 $Cu^{2+}$). These 12 Cu ions include two dimers, thus the fragment S contains $4.56 - 4.0 = 0.56$ free spins $Cu^{2+}$. By converting the unit into the fu, we get $2N_D = 4 \times 10/12 = 3.33$, and $N_F = 0.56 \times 10/12 = 0.478$, which is very close to the results for sample with $x = 0 (2N_D = 3.22, N_F = 0.43)$. For the compound with $x = 8.4$, the average $\alpha$ is $1.40 = 7/5$, as shown in figure 7. This value of $\alpha$ induces a slope $\tan\theta = 4/3$, as shown in figure 9(b). By cut and projection, the sequence is obtained as $LSSLSS\ldots$, and each pair of $LS$ is followed by a $S$ segment. In our model this means that every seven Cu ions have $3.8 \times 7/10 = 2.66$ $Cu^{2+}$, and include a dimer formed by two $Cu^{2+}$. So the excess segment $S$ induces 0.66 free spin $Cu^{2+}$. By converting the unit to the fu, we get $2N_D = 2 \times 10/7 = 2.86$ and $N_F = 0.66 \times 10/7 = 0.94$ in the formula unit, which accords with the experiment values ($2N_D = 2.78$, $N_F = 0.97$). Besides, this model can also explain the case of $\alpha$ greater than 10/7 for the oxygen nonstoichiometrical compounds [8]. For example, for $\alpha = 13/9$, the sequence is $LSLSLLSLSL\ldots$. Each 13 Cu ions contain two dimers. By using a total number of spins of 3.5 per fu [8], a similar calculation shows that $2N_D = 3.08$ and $N_F = 0.42$, which is the same as reported in [8]. Hence, we can conclude that the mismatch of the two sublattices, caused by either Ca doping or oxygen nonstoichiometry, induces a break up of the ideal sequence $LSLSLS\ldots$, and some dimers in spin chains can be decoupled into free spins $Cu^{2+}$. After Ca doping in the $Sr_{14}Cu_{24}O_{41}$ compounds, the lattice mismatch becomes larger. The larger mismatch will induce more dimers to be decoupled into free spins $Cu^{2+}$, but the total number of the $Cu^{2+}$ does not change.

As concerns the effect of Ca doping, it is seen that the magnetic properties and the lattice mismatch change as the Ca content changes, while the oxygen content is nearly fixed. This means that Ca substitution for Sr can change the magnetic property, no matter whether there is oxygen deficiency or not. The Ca doping has two effects. One is that it causes the loss of oxygen in the compound. Another is that it directly induces lattice misfit. Hence, the influence of Ca doping on the lattice misfit and the magnetic properties cannot simply be explained merely with oxygen deficiency. Second, from the viewpoint of microstructure, Sr layers are intercalated

between the $Cu_2O_3$ ladder and the $CuO_2$ chain layers. When Sr atoms are partially substituted by Ca, the electrostatic potential in the Sr layers will be changed. This change influences the $CuO_2$ chains, and as a result some segments are under tensile stress while others are under compressive stress. To satisfy the principle of minimum strain energy, lattice mismatch will occur. Therefore, the Ca-doped samples are not equivalent to the oxygen-deficient samples.

## 5. Summary

In this paper we studied the interplay between a modulated structure and the magnetic properties of the incommensurate composite crystal $Sr_{14-x}Ca_xCu_{24}O_{41}$, which has a complex structure with alternating layers containing $CuO_2$ chains and $Cu_2O_3$ ladders. For the Ca-doped $Sr_{14}Cu_{24}O_{41}$ compounds the characteristic decrease in the magnetic susceptibility below 80 K for pure $Sr_{14}Cu_{24}O_{41}$ compound disappears, and their magnetic susceptibility increases with increasing Ca content. This phenomenon is due to the change of $N_D$ and $N_F$ in the $CuO_2$ chain. The electron diffraction patterns show that the lattice mismatch along the chain direction between the two substructures increases with increasing Ca content. To understand the experimental results, we proposed a model by using a cut and projection method. Analyses show that the sequence of hole distribution of pure $Sr_{14}Cu_{24}O_{41}$ compound may be broken by Ca doping, and some dimers are decoupled into free spins.

## Acknowledgments

This work was supported financially by the National Natural Science Foundation of China (nos 10674105 and 50471028).

## References

[1] Dagotto E, Riera J and Scalapino D 1992 *Phys. Rev.* B **45** 5744
[2] Rice T M, Gopalan S and Sigrist M 1993 *Europhys. Lett.* **23** 445
[3] Abbamonte P, Blumberg G, Rusyd A, Gozar A, Evans P G, Siegrist T, Venema L, Eisaki H, Isaacs E D and Sawatzky G A 2004 *Nature* **431** 1078
[4] Kato M, Shiota K and Koike Y 1996 *Physica* C **258** 284
[5] Sigrist M, Rice T M and Zhang F C 1994 *Phys. Rev.* B **49** 12058
[6] Uehara M, Nagata T, Akimitsu J, Takahashi H, Mori N and Kinoshita K 1996 *J. Phys. Soc. Japan* **65** 1182
[7] McCarron E M, Subramanian M A, Calabrese J C and Harlow R L 1988 *Mater. Res. Bull.* **23** 1355
[8] Hiroi Z, Amelinckx S, Van Tendeloo G and Kobayashi N 1996 *Phys. Rev.* B **54** 15849
[9] Zimmermann M v, Geck J, Kiele S, Klingeler R and Buchner B 2006 *Phys. Rev.* B **73** 115121
[10] Amelinckx S and Van Dyck D 1992 Electron diffraction effects due to modulated structures *Electron Diffraction Techniques* vol 2, ed J M Cowley (Oxford: Oxford University Press) p 309
[11] Zeng Y, Shi J, Yu Z X and Pan F S 2005 *Mater. Lett.* **59** 662
[12] Azuma M, Hiroi Z, Takano M, Ishida K and Kitaoka Y 1994 *Phys. Rev. Lett.* **73** 3463
[13] Wu X-J, Takayama-Muromachi E, Suehara S and Horiuchi S 1991 *Acta Crystallogr.* A **47** 727
[14] Milat O, Van Tendeloo G, Amelinckx S, Mehbod M and Deltour R 1992 *Acta Crystallogr.* A **48** 618
[15] Takigawa M, Motoyama N, Eisaki H and Uchida S 1998 *Phys. Rev.* B **57** 1124
[16] Regnault L P, Boucher J P, Moudden H, Lorenzo J E, Hiess A, Ammerahl U, Dhalenne G and Revcolevschi A 1999 *Phys. Rev.* B **59** 1055
[17] Gotoh Y, Yamaguchi I, Takahashi Y, Akimoto J, Goto M, Onoda M, Fujino H, Nagata T and Akimitsu J 2003 *Phys. Rev.* B **68** 224108